frontiers in Marine Science

TYPE Original Research
PUBLISHED 06 May 2026
DOI 10.3389/fmars.2026.1733489

OPEN ACCESS

EDITED BY
Borja Aguiar-González,
University of Las Palmas de Gran Canaria, Spain

REVIEWED BY
Kathy Gunn,
Oceans and Atmosphere (CSIRO), Australia
Ricardo Matano,
Oregon State University, United States

*CORRESPONDENCE
Juliane U Wihsgott
jwi@pml.ac.uk

RECEIVED 27 October 2025
REVISED 30 March 2026
ACCEPTED 30 March 2026
PUBLISHED 06 May 2026

CITATION
Wihsgott JU, Palmer MR, Poulton AJ, Noyon M, Roberts M and Popova E (2026) Western boundary current - driven shelf sea deoxygenation on the Agulhas bank. *Front. Mar. Sci.* 13:1733489. doi: 10.3389/fmars.2026.1733489

Western boundary current - driven shelf sea deoxygenation on the Agulhas bank

Juliane U Wihsgott[1]*, Matthew R Palmer[1], Alex J Poulton[2], Margaux Noyon[3], Michael Roberts[3,4] and Ekaterina Popova[5]

[1]Plymouth Marine Laboratory, Prospect Place, Plymouth, United Kingdom, [2]The Lyell Centre for Earth and Marine Sciences, Heriot-Watt University, Edinburgh, United Kingdom, [3]Institute for Coastal and Marine Research, Nelson Mandela University, Gqeberha, South Africa, [4]School of Ocean and Earth Science, University of Southampton, Southampton, United Kingdom, [5]National Oceanography Centre, Southampton, United Kingdom

Dissolved oxygen is a fundamental component of healthy marine ecosystems and the livelihoods and economies they support. Despite its importance, dissolved oxygen is declining globally, and the processes driving deoxygenation in western boundary current systems remain poorly constrained. Here we present new autonomous ocean glider data from the eastern Agulhas Bank, a temperate shelf system off South Africa strongly influenced by the Agulhas Current. We identify a two-stage self-enhancing deoxygenation mechanism: shelf-edge exchange injects cold, nutrient-rich but oxygen-deficient South Indian Central Water onto the shelf, establishing and maintaining strong water column stratification; while wind-driven coastal upwelling fuels intense primary production and organic matter sinking that further enhances oxygen decline within the shelf sea interior. The first turbulence measurements in this region show that vertical mixing is too weak to sufficiently ventilate subsurface and near bed layers on the shelf, allowing low-oxygen conditions to persist. These results demonstrate that western boundary currents can precondition shelf seas for episodic oxygen depletion, with important implications for ecosystem resilience under projected climate-driven intensification of boundary current dynamics.

KEYWORDS
Agulhas current, biophysical-interactions, deoxygenation, oxygen dynamics, shelf edge exchange, western boundary current

1 Introduction

Dissolved oxygen concentrations are a key indicator of ecosystem health (Best et al., 2007) and climate change (Bopp et al., 2013; Oschlies et al., 2018). Global declines in dissolved oxygen have been observed since the 1960s (Stramma et al., 2008; Breitburg et al., 2018). These declines are widely attributed to global warming and nutrient enrichment in coastal waters (Schmidtko et al., 2017; Steckbauer et al., 2011) and are projected to accelerate with further climate change (Bopp et al., 2013; Diaz and Rosenberg, 2008; Oschlies et al., 2018). Oxygen decreases when demand from respiration and remineralisation exceeds physical and biological supply, leading to cascading effects from habitat compression to fishery collapse (Diaz and Rosenberg, 2008; Ekau et al., 2010). Hypoxia is widely defined as concentrations below 2 mg L^{-1} (approximately 64 µmol kg^{-1}), biological stress can occur at

higher concentrations (Vaquer-Sunyer and Duarte, 2008; Ekau et al., 2010), which is recognised in some regional shelf sea frameworks (e.g., OSPAR, 2017).

Eastern boundary upwelling systems are well known for coupling high coastal productivity with intense deoxygenation (Chavez and Messié, 2009; Breitburg et al., 2018; Luyten et al., 1983). They thus provide a useful framework for understanding how nutrient-rich, oxygen-poor waters impact adjacent shelves. Their source waters are oxygen-depleted due to long subsurface transit away from atmospheric ventilation (Luyten et al., 1983). When these preconditioned waters are brought to the surface by wind-driven upwelling, they deliver nutrients that fuel high primary productivity but also introduce low-oxygen conditions. Strong stratification further limits ventilation and amplifies oxygen loss through local uptake in the water column and sediments (Grantham et al., 2004; Diaz and Rosenberg, 2008). There is growing evidence that western boundary current systems can also experience significant deoxygenation events or even episodic hypoxia (Claret et al., 2018; Qian et al., 2017) despite their comparatively well-ventilated nature and their general role as barriers to lateral mixing (Stramma et al., 2008; Chavez and Messié, 2009). However, direct observational evidence linking western boundary current dynamics to shelf sea deoxygenation remains sparse.

The Agulhas Bank is a temperate shelf strongly influenced by the Agulhas Current (AC), the Southern Hemisphere's largest western boundary current (Krug et al., 2014). This provides an ideal setting for examining how western boundary-current interactions with the shelf contribute to shelf-sea oxygen dynamics. The Bank extends from 18°E to 29°E and forms a triangular extension of the South African continental shelf that is affected by both the Atlantic's Benguela Current and the Indian Ocean's AC (Chapman and Largier, 1989; Chapman and Shannon, 1987). It is considered a moderately productive system in the southern Indian Ocean (Mazwane et al., 2022), supporting major spawning grounds for numerous commercially important pelagic and demersal species, including anchovy, sardine, squid, hake and yellowtail (Hutchings, 1994). These fisheries play a crucial role in sustaining coastal livelihoods and contribute to regional food security (Chapman and Largier, 1989; Chapman and Shannon, 1987; Roberts, 2005).

Oxygen dynamics on the Agulhas Bank differ markedly between its western and eastern margins. West of 21°E Benguela upwelling dominates driven by equatorward trade winds (Boyer et al., 2001; Flynn et al., 2020). Hypoxic events are well documented here with the lowest bottom oxygen concentrations generally being found in this sector (Chapman and Shannon, 1987; Lovecchio et al., 2022; Roberts, 2005). In contrast, the eastern Bank, despite its ecological importance and productivity, oxygen dynamics here have received comparatively little attention. The region is generally described as well-oxygenated, although seasonal low-oxygen conditions have been observed, mostly in coastal areas (Chapman and Shannon, 1987; Roberts, 2005). Their drivers remain unclear (Giering et al., 2022), and to date no direct link has yet been established between deoxygenation and AC-driven exchange or to subsequent wind-driven processes. Given the AC's strong influence on shelf hydrodynamics, its role in shaping oxygen variability represents an important but unresolved question.

Flowing poleward along the Bank's eastern margin, the AC's position relative to the shelf strongly controls cross-shelf exchange (Leber et al., 2017; Malan et al., 2018). Interactions generate energetic exchanges, influenced by meanders and Natal Pulses, as well as sub-mesoscale cyclonic eddies and current-driven upwelling, the latter associated with intensified onshore Ekman transport within the frictional bottom boundary layer, known as Ekman veering (Jackson et al., 2012; Krug et al., 2014; Malan et al., 2018). These processes export shelf water offshore and episodically upwell cold, nutrient enriched South Indian Central Water (Leber et al., 2017; Lutjeharms et al., 1996, 2000) beneath a strong pycnocline which extends across much of the eastern Agulhas Bank (Swart and Largier, 1987). Wind-driven upwelling can then lift this water toward the surface and further distribute it across the shelf. Alongside these cold-water intrusions, the AC also delivers warm surface plumes and frontal features onto the eastern margin, further reinforcing stratification and influencing local productivity (Krug et al., 2014).

In this study, we use an integrated multi-platform observational approach to trace low-oxygen water masses from the shelf edge into the eastern Agulhas Bank. We identify a two-stage deoxygenation process: shelf edge exchanges introducing oxygen-depleted waters and establishing strong stratification, followed by localised upwelling that fuels high primary productivity; the subsequent remineralisation and respiration of sinking organic matter further reduces oxygen. This pathway highlights how climate-driven changes to boundary currents could accelerate regional deoxygenation, with important implications for ecosystem resilience (Oschlies et al., 2018; Bopp et al., 2013).

2 Methods

The observations presented here originate from the South African case study within the SOLSTICE-WIO programme (Sustainable Oceans, Livelihoods and Food Security Through Increased Capacity in Ecosystem Research in the Western Indian Ocean). The aim of this field study was to investigate ecosystem functioning on the eastern Agulhas Bank by integrating high-resolution *in-situ* observations with complementary Earth observation and reanalysis datasets. Ship-based CTD surveys and buoyancy driven ocean gliders collected new observations of temperature, chlorophyll-a (hereafter Chl-*a* and used as an indicator for phytoplankton biomass), dissolved oxygen and turbulent mixing across the eastern shelf. ERA5 reanalysis wind fields and satellite sea surface temperature composites provided regional context. Together, these datasets allowed us to link local processes to broader drivers of oxygen dynamics in this region.

2.1.Ship survey data

An across-shelf CTD survey was conducted aboard the R/V *Ellen Khuzwayo* (cruise EK188; Noyon, 2019) between 21 March and 2 April 2019. A total of 55 stations were sampled along 10 across-shelf transects (running from the nearshore to the shelf edge), numbered T01–12 from east to west. An additional transect

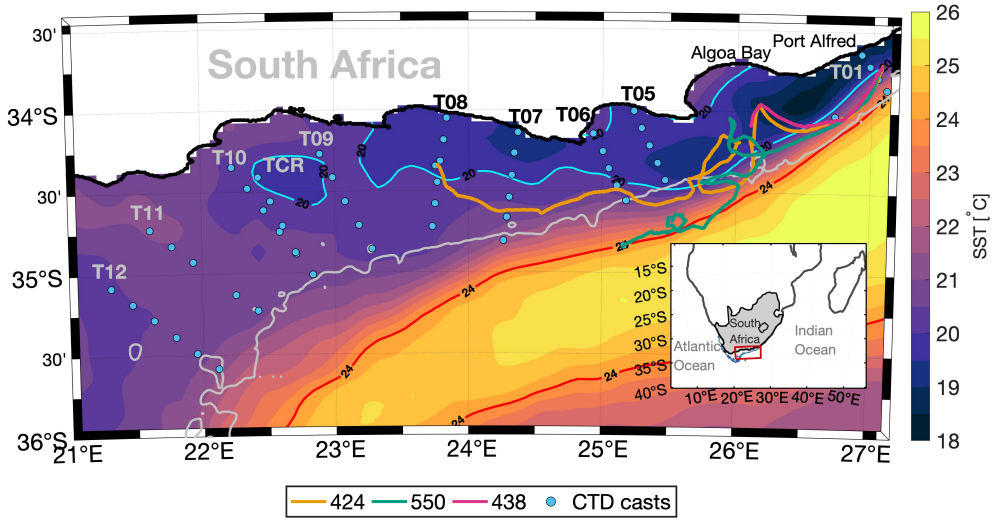

FIGURE 1
Map of ocean glider and CTD sampling locations on the eastern Agulhas Bank during March 2019. Background contours show SST [°C] data averaged over the duration of the field campaign, with the 20°C and 24°C isotherm highlighted in blue and red, respectively. The black and the grey contour mark the coast and 200 m isobath, respectively. The red box within the embedded map on the bottom right shows the study area within the wider context, with the 200 m isobath broadly outlining the Agulhas Bank south of South Africa.

(labelled "CR") and two full depth profiles at the recovery sites of ocean glider units 424 and 550 were also collected to aid instrument calibration (Figure 1). Poor weather conditions led to the early termination of transect 2 and the cancellation of transects 3 and 4.

At each station, vertical profiles of temperature, salinity, chlorophyll fluorescence and dissolved oxygen concentration were measured using a Sea-Bird 9plus conductivity-temperature-depth (CTD) instrument equipped with a Sea-Bird SBE 43 dissolved oxygen sensor and Sea-Bird ECO Triplet Fluorometer, mounted on a 12-bottle rosette sampling system. Dissolved oxygen profiles were calibrated against Winkler titration samples collected from CTD Niskin bottles and analysed onboard according to GO-SHIP international protocols (Langdon, 2010). Discrete Chl-*a* [mg m^{-3}] measurements were also collected from Niskin bottles, with measurements performed using a Turner Trilogy Instrument (Poulton et al., 2022) and used to calibrate the CTD fluorometer. All CTD data were processed and quality-controlled using SeaBird software (Seasave version 7.26.7), with manual de-spiking of anomalies in regions of strong gradients, and averaging onto a 1 dB vertical grid, as described in the accompanying metadata (see Data Availability).

Shipboard and lowered acoustic Doppler current profiler data, as well as onboard meteorological measurements were unavailable for this cruise due to instrument failure. As a result, we were unable to directly measure *in-situ* horizontal current velocities or local wind conditions from the vessel during EK188.

2.2 Ocean glider data

To track upwelled water and characterise oxygen dynamics across the study region, three buoyancy-driven ocean gliders (units 424, 438, and 550) were deployed. Units 424 and 438 were Teledyne Webb Slocum G2 gliders, equipped with thrusters to assist propulsion when necessary, unit 550 was a Kongsberg M1 Seaglider. All gliders were deployed at the same site in approximately 90 m water depth, roughly 20 km southwest of Port Alfred (Figure 1; Supplementary Figure S1) and later recovered by the R/V Ellen Khuzwayo. Sensor setups, and full deployment and recovery details are summarised in Table 1.

This mission posed significant challenges to the predominantly buoyancy driven vehicles due to strong sub-mesoscale currents and shelf edge dynamics. Our intended sampling strategy was to conduct several across-shelf (zigzag) transects between the 75 m coastal isobath and the shelf edge while being advected by the predominant westerly currents parallel to the shelf edge (Boyd and

TABLE 1 Summary of specifications of the three buoyancy-driven ocean gliders, including model type, sensor setup, and deployment/recovery positions.

Glider unit	Model and depth rating	Science sensors	Deployment date & location	Recovery date & location
424	Slocum G2 200 m rated	GPCTD, Aanderaa optode, Rockland MicroRider	14th March 2019, 26.950°E, 33.633° S	31st March 2019, 23.756°E, 34.346°S
438	Slocum G2 200 m rated	GPCTD, Aanderaa O_2 optode, ECO Triplet (Chl-*a*)	14th March 2019, same site	25th March 2019, 25.531°E, 34.155°S
550	Seaglider M1, 1000 m rated	GPCTD, Aanderaa O_2 optode, ECO Triplet (Chl-*a*)	14th March 2019, same site	31st March 2019, 24.932°E, 34.923°S

Shillington, 1994; Swart and Largier, 1987). The combination of shallow diving depths, wind driven circulation close to the coast and localised sub-mesoscale features (including eddies and strong currents in excess of 1 m s^{-1} in the vicinity of the AC) hindered this sampling strategy. At times, only the use of thrusters fitted on units 424 and 438 enabled the continuation of the planned cross-shelf transects (Figure 1; Supplementary Figure S1).

Following the correction of all science and navigational data using established oceanographic methods (Lueck and Picklo, 1990; Garau et al., 2011; Bittig et al., 2014) we applied factory calibrations to all science sensors. We then corrected all observations (except measurements and derived products of turbulent shear) for sensors offsets and drifts by calibrating against co-located, calibrated profile and bottle data collected during the EK188 survey or cross calibrating against alongside glider observations.

2.2.1 Turbulence methods

Turbulent kinetic energy dissipation (ε) was estimated from microstructure measurements collected by the Rockland Scientific MicroRider mounted on the upper forward section of the glider 424. The MicroRider contained two forward facing shear probes and ε [W kg^{-1}] was derived following Palmer et al. (2015). The vibration of an active thruster introduced low frequency noise that had a detrimental impact on shear spectra. Thus, only shear and derived ε data from periods when the thruster was not operational were included in our analysis.

To quantify diapycnal mixing across the shelf, we estimated the vertical turbulent diffusion rate at the base of the euphotic zone, K_z [m^2 s^{-1}], using the Osborn relation:

$$K_z = \Gamma \frac{\varepsilon}{N^2}$$

where ε is the turbulent kinetic energy dissipation rate [W kg^{-1}], N is the Brunt-Väisälä buoyancy frequency [s^{-1}] (calculated from the coincident density profile by unit 424), and Γ is the mixing efficiency, commonly assumed to be 0.2 (Gregg et al., 2018). While some debate remains over the exact value of diapycnal mixing efficiency in weakly energetic regimes (Monismith et al., 2018), in the dynamic waters of the Agulhas Bank we follow the standard convention by assuming a mixing efficiency of 0.2 (Osborn, 1980). The Brunt-Väisälä frequency, N, was calculated using the density profile from unit 424 as follows:

$$N^2 = -\frac{g}{\rho}\left(\frac{\partial \rho}{\partial z}\right)$$

where g [m s^{-2}] is gravitational acceleration, ρ is density [kg m^{-3}], and z is depth [m]. Given the broad and complex pycnocline observed across the eastern Agulhas Bank, maintained by strong advective processes (Boyd and Shillington, 1994; Hutchings, 1994) a single sharp interface, often present in temperate shelf seas that separates water masses with differing dissolved oxygen or nutrient characteristics could not be identified. Consequently, because no single, dominant density interface could be defined we did not derive K_z at a fixed pycnocline depth. Instead and consistent with our focus on quantifying diapycnal fluxes relevant to biological production and bottom–layer ventilation, we calculated a representative value at the base of the euphotic zone, Z_{Eup} = 30 ± 6 m (Poulton et al., 2022), and define this value as K_{eup}, an indicator of vertical exchange relevant for biological production and ventilation processes.

To identify the role of diapycnal mixing during stratified conditions, we included only observations with N^2 ≥1 x10^{-4} s^{-2}, excluding well-mixed regions to restrict the analysis to periods of meaningful vertical stratification. The complex current dynamics on the shelf required intermittent use of the thruster throughout the deployment, which limiting continuous ε measurements. Thus, we report the deployment mean of K_{eup} over the sampled shelf area.

2.3.Reanalysis wind data

To assess wind forcing, we used ERA5 reanalysis of 10 m wind vectors (u, v) [m s^{-1}], sourced from the Copernicus Climate Change Service (Hersbach et al., 2018). ERA5 was selected for its high spatial (~37 km) and temporal (hourly) resolution, which is important to resolve wind variability associated with coastal orography and sharp sea surface temperature gradients in the study region. Hourly data spanning 14 March (00:00) to 2 April (23:00) 2019 were extracted for the domain 21.00–27.25°E, 33.40–36.00°S.

Wind stress was calculated as $\tau = c_d \rho_a u^2$ with air density ρ_a = 1.225 kg m^{-3} and drag coefficient c_d = 1.25 x 10^{-3} (Kara et al., 2007). Wind stress curl was then calculated as: $\nabla \times \tau = \frac{\partial \tau_y}{\partial x} - \frac{\partial \tau_x}{\partial y}$ [N m^{-3}], where τ_x and τ_y [N m^{-2}] are the zonal and meridional wind stress components. Ekman pumping velocities were calculated using the classical formulation (Gill, 1982): $w_E = \frac{1}{\rho f}\left(\frac{\partial \tau_y}{\partial x} - \frac{\partial \tau_x}{\partial y}\right)$, where f is the Coriolis parameter. While alternative formulations include an additional planetary vorticity gradient correction (e.g., Bravo et al., 2016), the classical formulation used here is appropriate for regional studies such as ours. In the Southern Hemisphere, negative (positive) wind stress curl indicates a divergent (convergent) wind field, associated with upwelling (downwelling) (Gill, 1982).

2.4 Sea surface temperature data

Daily sea surface temperature composites were obtained from the UK Met Office's Operational Sea Surface Temperature and Sea Ice Analysis (OSTIA), which provides daily, gap-free foundation sea surface temperature at 0.05° resolution by assimilating *in-situ* and satellite data from infra-red and microwave radiometers (Good et al., 2020), accessed via the Copernicus Marine Environment Monitoring Service (CMEMS). The dataset spans 1 March to 3 April 2019, covering 17–28°E and 33–38°S.

3 Results

3.1 Regional hydrographic conditions

New data from autonomous ocean gliders and ship-based surveys collected during the March 2019 field campaign provide detailed insights into hydrographic structure, oxygen dynamics and Chl-*a* distributions on the eastern Agulhas Bank. To place these observations in the wider regional context, Figure 1 presents CTD

sampling locations alongside glider surface positions moving from east to west, overlaid on OSTIA sea surface temperature (SST, °C) observations averaged over the March 2019 field campaign.

Warmer waters (24 °C isotherm, highlighted red in Figure 1) outline the south-westward flowing AC. It generally flowed along the shelf edge (200 m isobath), and remained in a non-meandering state along the eastern Agulhas Bank during the field campaign. Elevated shelf SSTs near the 200 m isobath around 26.50–27.00°E indicate that the current was close to the shelf edge in this region. In contrast, relatively cooler SSTs (< 20 °C isotherm in Figure 1) occupied almost the whole shelf between 25.50°E and 27.00°E but farther west they were confined to coastal stations between 23.25°E and 25.50°E, where the shelf starts to widen at 25.5.

3.2 Wind forcing during the field campaign

ERA5 reanalysis data show that 10 m wind speeds averaged 5.3 ± 2.9 m s^{-1} across the eastern Agulhas Bank throughout the observational period, with episodic stronger events. Wind directions were predominantly alongshore and characterised by some mesoscale variability off the shelf. Winds alternated between easterly, driving offshore Ekman transport and thus promoting coastal upwelling, and westerly driving onshore transport linked to coastal downwelling.

Spatial variability in the daily averaged wind stress field and its curl ($\nabla \times \tau$ [N m^{-3}]) provides an additional mechanism for coastal upwelling (Rykaczewski and Checkley, 2008; Pickett and Paduan, 2003), driven by orography and large SST gradients or fronts (Akpinar et al., 2022; Chelton et al., 2004; Wang and Castelao, 2016), both of which are prevalent around the eastern Agulhas Bank (Figure 1). The intensity of negative wind stress curl varied in space and time, with several strong pulses of clockwise-rotating (spatially diverging) fields lasting multiple days over the eastern Agulhas Bank.

3.3 Agulhas current-intrusions and density stratification

Figure 2 shows high-resolution glider observations collected along the westerly transect across the eastern Agulhas Bank. These reveal several instances of active upwelling onto the shelf edge of the eastern Agulhas Bank, indicated by the uplift of the γ = 26.7-26.8 neutral density surfaces (Figure 2a), showing vertical displacement of offshore South Indian Central Water (SICW) on the continental shelf (Leber et al., 2017; Lutjeharms et al., 1996). Notable events occurred during decimal days 81–83 farther east near ~26°E, and were supported by CTD transects T05 and T06 (Figures 3h, i). A smaller uplift of the isopycnals was also visible around decimal days 76–77 as the glider crossed the shelf break, although this feature was less pronounced than the later event. These events are clearly identifiable by steeply sloping isopycnals as the gliders travels over the shelf break (Figure 2a). Near–bottom waters during these events reached ~8 °C (Lutjeharms et al., 1996), indicating the presence of cooler offshore waters being uplifted onto the shelf. The isopycnal heave observed

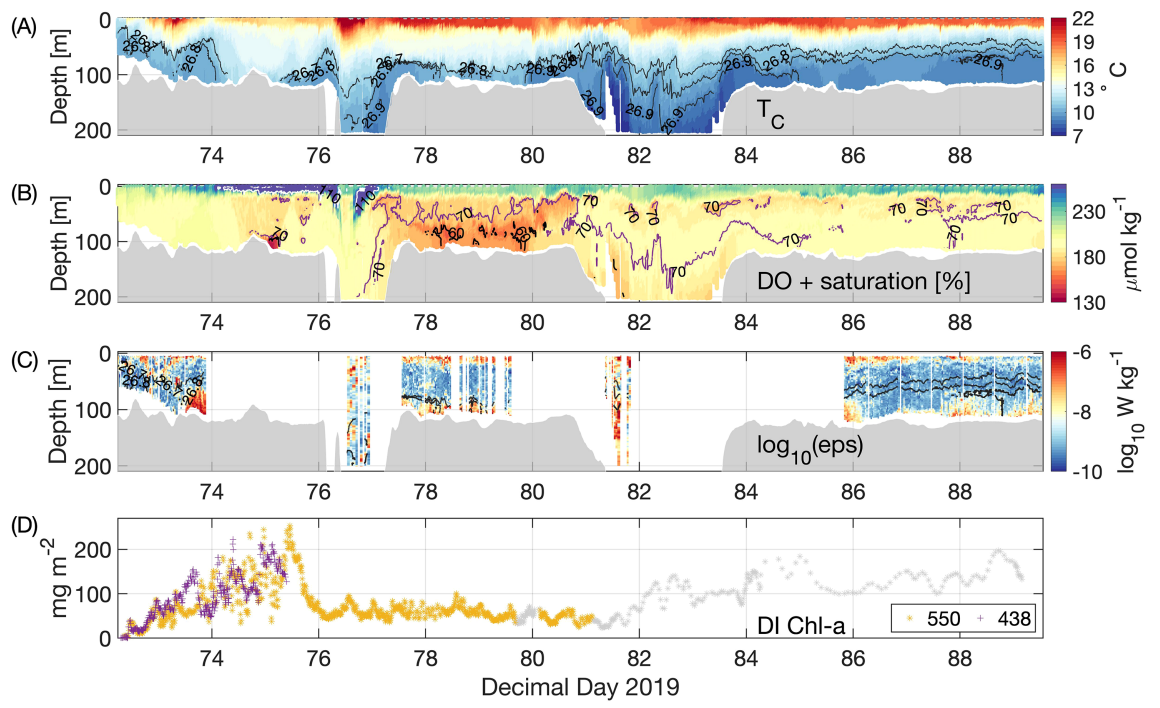

FIGURE 2
Glider observations: **(A–C)** Data from glider 424: **(A)** Conservative temperature [°C] with overlaid neutral density isopycnals [γ = 26.7–26.9]; **(B)** dissolved oxygen concentrations [µmol kg^{-1}] with saturation contours at 60%, 70%, and 110%; **(C)** Turbulent kinetic energy (TKE) dissipation rate [$\log_{10}\varepsilon$, W kg^{-1}], overlaid with the same isopycnals. The grey shaded area beneath each panel shows the interpolated seabed from GEBCO bathymetry. **(D)** Depth-integrated Chl-a biomass [mg m^{-2}] from gliders 550 and 438. Yellow stars and purple crosses indicate shelf-based values from gliders 550 and 438, respectively. Grey markers represent values from glider 550 beyond the shelf break. Temporally referenced glider locations for all units are provided in Supplementary Figure S1.

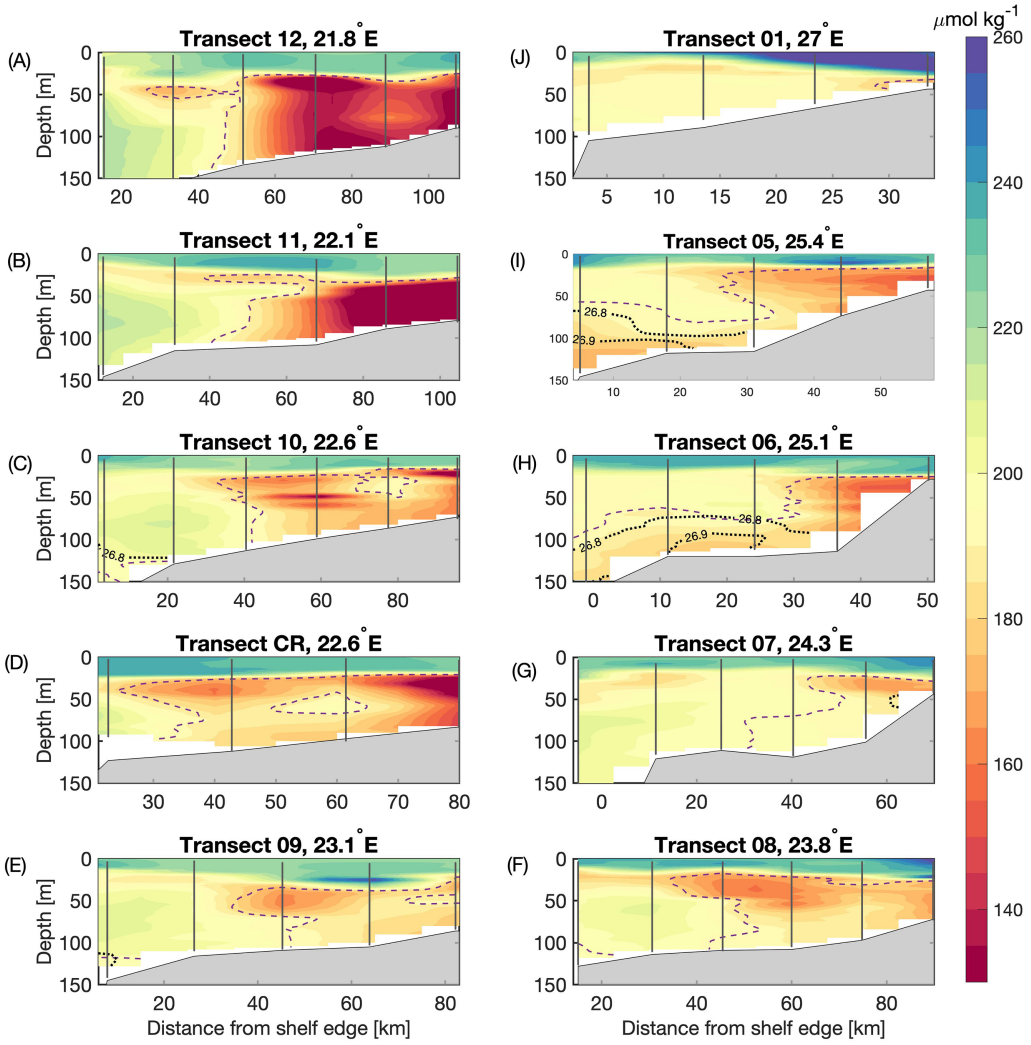

FIGURE 3
Cross-shelf observations of dissolved oxygen [μmol kg^{-1}] collected during CTD transects 12-1 [referenced **(A–J)**] from west to east. Neutral density isopycnals [γ = 26.8–26.9] are overlaid (black dotted), together with the 70% oxygen saturation contour (magenta dashed). Vertical lines mark CTD stations, and grey shading denotes the seabed from CTD altimeter data.

across the shelf break is consistent with SICW intrusion onto the shelf as proposed by Leber et al. (2017) & Lutjeharms et al. (1996).

Vertical stratification strengthened westward across the transect. Glider profiles showed that the top–to–bottom temperature difference increased almost linearly from 1.55 °C at 27°E to a local maximum of 9.55 °C at 24°E (Figure 2a). This corresponds to a mean increase of ~0.33 °C per day in vertical temperature difference, with some deviations from a linear trend. The distribution of density surfaces and the observed westward intensification of vertical gradients highlight the presence of cold, dense water at depth beneath warmer surface layers. These features were most pronounced near the shelf edge and diminished farther inshore.

3.4 Turbulence and vertical mixing

Direct measurements of TKE dissipation rates (ε) were obtained for the eastern Agulhas Bank for the first time (Figure 2c). Elevated values of ε (> 10^{-6} W kg^{-1}) were mostly confined to episodic events within the surface and bottom boundary layers. In contrast, mid–water ε values remained generally low (O 10^{-9} W kg^{-1}), likely due to a broad and complex pycnocline. Conservative temperature profiles (Figure 2a. Supplementary Figures S2a, S3a) indicate a gradual temperature/density transition rather than a single sharp interface, which inhibits turbulent mixing except in isolated regions near the AC, at or beyond the shelf edge (Figure 2c).

Temperature profiles revealed high-frequency oscillations (Figure 2a), indicative of internal wave activity. To assess the overall importance of diapycnal mixing, vertical turbulent diffusion rates were calculated at the base of the euphotic zone (K_{eup}; see Section 2.2). The average K_{eup} was 7.6×10^{-6} m^2 s^{-1} ($\pm$ 4.7×10^{-6}, 95% CI), with variability spanning three orders of magnitude.

3.5 Oxygen distribution and vertical gradients

Glider and CTD profiles showed pronounced vertical oxygen gradients across the eastern Agulhas Bank. Oxygen concentrations in the upper 50 m remained relatively high (> 230 μmol kg^{-1}), with

local maxima reaching up to 391 μmol kg^{-1}, equivalent to 150% oxygen saturation. Persistently high values above 110% oxygen saturation were also evident across the region (Figure 2b; Supplementary Figure S2c), especially in the upper 10 meters within the Algoa Bay region around decimal day 75, and in some areas extending to depths of 40 meters in the vicinity of the AC (Figure 2b).

Below the pycnocline, relatively low oxygen concentrations were observed of around ~190 μmol kg^{-1} (≈70 % saturation) associated with the SICW intrusions described in Section 3.3 and indicative of water that has not been recently ventilated or that has undergone oxygen consumption. These moderately oxygen–deficient layers were broadly distributed across the shelf in both glider and CTD profiles. Across the study region, over 80% of glider profiles and 90% of CTD casts recorded values at or below 70% saturation (magenta contour Figures 2b, 3; Supplementary Figures S2c, S3c). Farther west along the glider transect, concentrations declined further, with minimum values of ~120 μmol kg^{-1} recorded locally at depths of 80–120 m (Figure 2b; Supplementary Figures S2c, S3c). The lowest values were seen away from the shelf edge around decimal day 75.

Inshore profiles generally showed comparatively higher concentrations, whereas shelf–edge profiles exhibited steeper declines with depth. CTD transects T05 and T06 showed similar patterns, with near–bottom oxygen concentrations consistently lower than mid–water values (Figures 3h, i). Overall, the westward intensification of vertical oxygen gradients matched the strengthening thermal and density stratification described in Section 3.3.

3.6 Chlorophyll structure and phytoplankton biomass

Glider and CTD Chl-*a* measurements revealed clear vertical structure and spatial gradients in phytoplankton biomass across the eastern Agulhas Bank. Concentrations in the upper 10–20 m were generally elevated, often exceeding 5 mg m^{-3} (Supplementary Figures S2b, S3b). Peak values from glider units 438 and 550 reached > 25 mg m^{-3} in the upper water column, particularly south of Algoa Bay where stratification was relatively weak. A subsurface chlorophyll maximum (SCM, defined as subsurface Chl-*a* > 1.5× surface values following Poulton et al., 2022) was detected in 21% of on–shelf glider profiles.

4 Discussion

4.1 Stage 1: Current driven upwelling and physical preconditioning

High–resolution glider and CTD observations revealed repeated uplift of neutral density surfaces (γ = 26.7–26.8) along the eastern Agulhas Bank, accompanied by relatively cool (~8 °C) near–bed (i.e. within the bottom mixed layer) advection. These features indicate a direct connection between off-shelf and on-shelf waters, and we infer that they reflect the upwelling of SICW along the shelf edge. The clearest uplift event during the deployment was observed between decimal 81–83 near ~26°E, supported by CTD transects T05 and T06 (Figures 3h, i). A smaller uplift of the isopycnals was also visible around decimal days 76–77 as the glider crossed the shelf break, although this feature was less pronounced than the later event. The localised presence of γ = 26.7–26.8 surfaces near the shelf edge, and their absence farther inshore, is more consistent with current-induced upwelling events than with lateral advection of cold shelf waters. A semi-permanent upwelling cell is frequently observed off Port Alfred (Jackson et al., 2012; Lutjeharms et al., 2000), and the timing and location of the uplift events documented here align with this feature. Satellite SST fields during the field campaign show a stable AC path along the shelf edge, with the 24 °C isotherm closely following the 200 m isobath (Figure 1). Large Agulhas meanders occur episodically, often with only one or two major events per year (Krug and Penven, 2011; Beal et al., 2015), so the non–meandering configuration observed here is representative of the prevailing shelf–edge circulation and provides insight into typical exchange processes between the Agulhas Current and the eastern Agulhas Bank.

The westward intensification of vertical temperature differences, with top-to-bottom gradients increasing from ~1.5 °C at 27°E to over 9 °C at 24°E, highlights the role of current-driven intrusions in shaping stratification across the shelf. These features were strongest near the shelf edge and weakened inshore, reflecting spatial variability in Agulhas Current-shelf exchange. After upwelling, SICW occupies deep layers on the shelf, reinforcing vertical density gradients along the westward transect. While seasonal surface-driven buoyancy forcing increases stratification across all shelf systems, the intrusion of cold, dense SICW from below broadens the pycnocline, generating the diffuse structure observed across the eastern Agulhas Bank.

SICW is not only cold but also relatively low in dissolved oxygen, with concentrations of around 190 μmol kg^{-1} (approximately 70% oxygen saturation) (Figure 2b; Supplementary Figures S2c, S3c). This value is at the thresholds recognised in regional frameworks as *oxygen deficiency* (Mahaffey et al., 2020; Painting et al., 2005), indicating that the water entering the shelf is already preconditioned with moderately low oxygen water. Using this definition, oxygen deficiency was common across the shelf, with over 90% of CTD casts and over 80% of 3,308 glider profiles recorded concentrations below 190 μmol kg^{-1}. Rather than being confined to near–bottom waters, as previously assumed (Chapman and Shannon, 1987), the most depleted layers often occurred at mid–depths, reflecting both the shelf–edge advection of oxygen–poor water and likely secondary processes that further lift and intensify this signal, such as respiration and remineralisation of sinking organic matter following *in-situ* growth.

Turbulent mixing across stratified layers (diapycnal mixing) is often considered a critical control on the vertical distribution of temperature, oxygen, and nutrients in shelf seas and the open ocean (Oschlies et al., 2018; Rippeth et al., 2024). It enables the upward flux of nutrients into the euphotic zone that fuels primary production and oxygen generation, while simultaneously ventilating layers beneath the pycnocline (Townsend et al., 2006; Williams et al., 2022). Here we assess the contribution of diapycnal mixing to the observed patterns. Our observations indicate that mixing on the eastern Agulhas Bank was generally weak (O10^{-9} W kg^{-1}). Elevated

dissipation ($\varepsilon > 10^{-6}$ W kg^{-1}) was restricted to boundary layers and intermittent events, while the interior remained strongly stratified. This suggests that the broad pycnocline acted as an effective barrier to vertical exchange, limiting the capacity of turbulence to ventilate the bottom mixed layer.

Processes such as tides, wind forcing, and internal waves are known to enhance mixing in other shelf systems (Sharples et al., 2001; Moore et al., 2003), and signatures of internal wave activity were evident in temperature profiles. Here, however, their contribution appeared limited over the observational period sampled. Vertical turbulent diffusion rates at the base of the euphotic zone averaged 7.6×10^{-6} m^2 s^{-1} ($\pm$ 4.7×10^{-6}, 95% CI), an order of magnitude lower than typical shelf values (e.g., Sharples et al., 2001; MacKinnon and Gregg, 2005) and those reported for the global ocean (Waterhouse et al., 2014). Although highly variable across three orders of magnitude, these values were insufficient to overcome the strong stratification imposed by current–driven exchanges. As a result, diapycnal mixing could not ventilate the bottom mixed layer, reinforcing vertical gradients in both temperature and dissolved oxygen. In contrast, wind–driven coastal upwelling, is a primary route for supplying nutrients into the euphotic zone (Largier and Swart, 1987; Lutjeharms et al., 2000), supported by the rough coastline and prevailing easterly winds typical of the region during the austral summer (October–March) (Boyd and Shillington, 1994; Probyn et al., 1994). These conditions establish a strongly stratified and oxygen–limited shelf environment, setting the stage for the episodic wind–driven amplification described in Stage 2.

4.2 Stage 2: Wind-driven forcing and biological amplification

While current–driven intrusions strongly influence stratification at the shelf edge, wind forcing provides an additional mechanism that modulates vertical density structure across the Agulhas Bank. Alternating easterly and westerly regimes drove intermittent coastal upwelling and downwelling. The strongest biogeochemical impacts were associated with episodes of negative wind stress curl, most notably around decimal days 74–76 when moderate easterlies combined with strong negative curl to generate upwelling –favourable conditions (Figure 4a). During this period the 20 °C isotherm lay close to the coast, closely aligned with negative peaks in wind stress curl (Figures 4a, b). Time series of wind and SST averaged south of Algoa Bay (Figures 4c, d), where the gliders were sampling during this event, indicate that the most pronounced cooling likely preceded the glider transects, suggesting that the upwelling event was part of a longer sequence of wind-driven forcing. Nevertheless, the oxygen supersaturation in surface waters (up to 192%) during the glider deployment indicates a sustained biological response to the earlier upwelling of cold, nutrient-rich waters (Giering et al., 2022). Ekman pumping estimates suggest vertical velocities of up to 3.0 m day^{-1} locally, with regional averages of ~1.5 m day^{-1}. While these values fall within ranges reported in some Eastern Boundary Upwelling systems (e.g., Halpern, 2002; Bravo et al., 2016), wind curl driven pumping is likely to play a supporting, secondary role here compared to coastal Ekman upwelling. High nutrient availability in the euphotic zone fueled enhanced primary production, with Chl-*a* concentrations exceeding 25 mg m^{-3} in the upper water column, particularly south of Algoa Bay where stratification was relatively weak (Supplementary Figures S2b, S3b). To distinguish whether elevated surface Chl-*a* reflected *in-situ* phytoplankton growth or simply vertical redistribution, we examined depth-integrated Chl-*a* biomass from glider units 550 and 438 (Figure 2d). Integrated biomass peaked at 250 mg m^{-2} near decimal day 75.5, coinciding with oxygen supersaturation (up to 192%) in surface waters. Together, these peaks support the interpretation that local phytoplankton growth, rather than redistribution, drove the observed oxygen enrichment.

Shortly after this event, the lowest dissolved oxygen concentrations were observed in bottom–layer inshore waters (~119 µmol kg^{-1}; 45% saturation, Supplementary Figure S2). This minimum approaches critical thresholds for several pelagic species (Ekau et al., 2010; Roberts, 2005), including regionally important cephalopods that have experienced catch crashes in recent decades (Jebri et al., 2022). Notably, this minimum was only detected by ocean gliders operating throughout severe weather conditions, which prevented completion of ship-based CTD transects T2–4 in this area (Noyon, 2019). This highlights a potential bias in historic observations that often lack measurements during strong winds, a persistent feature of the Agulhas Bank region and other temperate and high-latitude shelf seas. The coastal location of the observed dissolved oxygen minimum also illustrate how high coastal productivity can promote enhanced oxygen consumption within interior waters through the accumulation and sinking of particulate organic matter and increased microbial respiration, a pattern consistent with other strong upwelling regions (Chavez and Messié, 2009; Breitburg et al., 2018).

SCMs are a common feature in summer–stratified shelf seas, where phytoplankton optimise growth at the thermocline by accessing nutrient fluxes from below while adapting to low light conditions (Hickman et al., 2012; Williams et al., 2022). On the Agulhas Bank, SCMs have previously been reported as a characteristic summer feature, linked to strong stratification and considered important for zooplankton feeding and fish spawning success (Lutjeharms et al., 1996, Probyn et al., 1994). Based on CTD observations from the EK188 cruise, Poulton et al. (2022) found SCMs at 47% of stations across the Bank and noted a westward deepening of the feature. In contrast, SCMs were detected in only 21% of on–shelf glider profiles during our deployment. This reduced occurrence, together with elevated surface–integrated biomass, indicates that physical upwelling supplied nutrients directly into the surface layer, favouring in–situ surface production over diapycnal mixing based SCM formation.

The link between high nutrient levels and low dissolved oxygen on the eastern Agulhas Bank has received little attention in previous investigations, likely due to the apparent lack of direct connectivity between upwelling events and observed areas of oxygen depletion. On the eastern Agulhas Bank, initially upwelled water only exhibits moderately reduced dissolved oxygen at the shelf edge and may not have been considered a cause for concern. The strong vertical density gradient maintained at the shelf break can inhibit vertical exchange and prevent the biological utilisation of nutrient-enriched

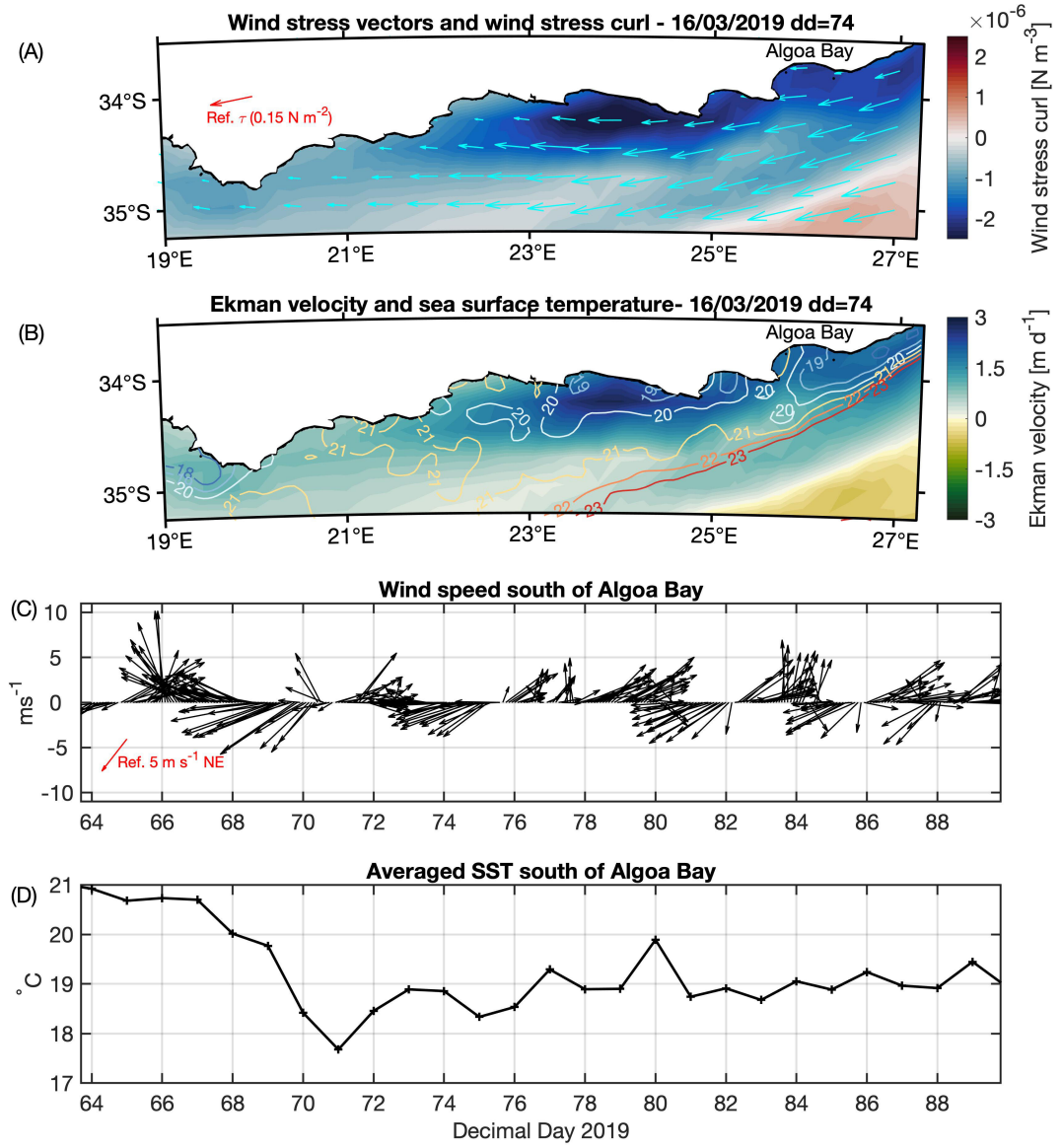

FIGURE 4
Wind driven upwelling. **(A)** Wind stress (cyan arrows) and wind stress curl [N m^{-3}]; note that negative curl indicates divergence and upwelling. A red reference arrow indicates the wind stress corresponding to a 10 m s^{-1} wind from 80°. **(B)** Daily averaged Ekman velocity [m d^{-1}]; positive values indicate upwelling with overlaid contours of SST. **(C)** Daily averaged wind speed [m s^{-1}] and SST [°C] data south of Algoa Bay, highlighting cooling associated with northeasterly, diverging winds driving coastal upwelling. A reference arrow in **(C)** indicates a 5 m s^{-1} wind speed from the northeast.

waters until they are upwelled at the coast, some distance and time after initially being transported onto the Agulhas Bank.

All productive shelf seas at temperate latitudes experience gradual deoxygenation below the pycnocline during the seasonal cycle that begins with the onset of spring stratification (Fennel and Testa, 2019; Wei et al., 2019; Williams et al., 2022; Yu et al., 2015). Most, however, undergo complete vertical mixing in winter, ventilating the whole water column, and resetting dissolved oxygen to saturated levels ahead of the next season. In contrast, the eastern Agulhas Bank appears capable of maintaining stratification in some offshore areas during austral summer (Swart and Largier, 1987). AC-driven shelf-edge upwelling combined with low diapycnal diffusivity may limit complete mixing and thus ventilation, allowing low dissolved oxygen to persist in interior waters intermittently. While observed dissolved oxygen minima do not reach hypoxic levels, the combination of stratification, nutrient supply, and episodic upwelling suggests that the eastern Agulhas Bank could be vulnerable to oxygen reduction during periods of prolonged stratification or weak advective transport. Residence times, and thus oxygen depletion risk, depend on the current's position relative to the shelf: meanders closer to the shelf slow flow and lengthen residence times, while offshore positions accelerate transport (Boyd and Shillington, 1994; Jackson et al., 2012; Malan et al., 2018).

4.3 Broader controls on oxygen dynamics and shelf vulnerability

Our results highlight a fundamental distinction between vertical mixing and advective upwelling on the eastern Agulhas Bank. Diapycnal mixing acts as a two-way conduit, simultaneously

supplying nutrients to the surface and ventilating the bottom mixed layer. In contrast, the upwelling we observed acts largely in a one-way sense advecting subsurface waters onto the shelf and into the euphotic zone, reinforcing vertical gradients in oxygen and supporting localised primary production. Together these processes demonstrate how AC-driven shelf-edge upwelling preconditions the shelf with cold, nutrient-rich, and moderately low oxygen water, while wind-driven upwelling enables its biological utilisation further inshore and simultaneously amplifies the reduction of dissolved oxygen within interior waters. This distinction explains why episodic wind-driven upwelling produces strong vertical gradients in dissolved oxygen, while background mixing and advective transport moderate their persistence.

Subsequent ventilation with the surface layer is prevented by strong and persistent stratification, which itself is maintained by the same cool, nutrient-enriched waters that fuel productivity. Upwelled waters fuel bursts of primary production that, while enhancing surface oxygen supersaturation, also drive oxygen drawdown in interior waters via particulate organic matter export and microbial respiration (Giering et al., 2022). The observed bottom-layer minimum (~119.7 μmol kg^{-1}; 45% saturation) approaches thresholds for some pelagic species (Roberts, 2005), highlighting the ecological and potentially socio-economic significance of these events (Jebri et al., 2022). Upwelling in this system thus not only preconditions the shelf with moderately low oxygen water but also primes coastal waters to further deoxygenate to promote the creation of oxygen depletion zones within the eastern Agulhas Bank interior.

Understanding changes to shelf-edge and coastal upwelling and the tightly linked seasonality of stratification on the eastern Agulhas Bank, is central to understanding how the regional oxygen inventory and ecosystem health will respond to future changes. The generation and expansion of such oxygen-deficient regions could, in the short term, present opportunities for local fishing communities as habitats become compressed due to area avoidance (Breitburg et al., 2018). In the medium to long term however, these findings present an early warning for the southern AC upwelling region. Although observed concentrations do not reach hypoxic levels the physical conditions of the eastern Agulhas Bank promote further depletion of dissolved oxygen within coastal regions, highlighting the sensitivity of this system to changes in stratification, residence time and advective transport.

Current evidence suggests that the regional effects of future climate change could amplify the oxygen depletion on the eastern Agulhas Bank. The reported broadening of the AC (Beal and Elipot, 2016) is likely to intensify shelf edge exchange, potentially further strengthen stratification across the Bank, and increasing both the nutrient load onto the shelf (Jury, 2020; Malan et al., 2018) and the subsequent production of organic matter. Ocean warming will reduce the solubility of dissolved oxygen and accelerate respiration rates (Breitburg et al., 2018). At the same time, stronger vertical stratification will further restrict vertical mixing, limit ventilation and allow strong oxygen gradients to persist. The cumulative impacts of these future changes, coupled with the current state of coastal waters reported here therefore provides cause for concern for the marine ecosystems of the eastern Agulhas Bank and the communities dependent on this currently rich natural resource.

5 Conclusions

This study provides the first direct evidence that Agulhas Current-driven shelf edge exchange and localised upwelling can jointly drive a two-stage deoxygenation process on the eastern Agulhas Bank. These results include the first direct turbulence measurements for the eastern Agulhas Bank, offering new constraints on vertical exchange processes that underpin oxygen dynamics in this region. These insights improve our understanding of the dominant drivers of oxygen loss in shelf seas influenced by western boundary currents and will inform models predicting climate-change impacts on ecosystem health and food security. To validate these predictions, increased monitoring over a range of temporal and spatial scales is required as many questions remain. Although our glider deployment covered only a 16–day period, it captured the open–ocean to shelf–edge intrusion of SICW that underpins the two–stage deoxygenation process, highlighting the value of sustained high–frequency observations on the eastern Agulhas Bank. Autonomous ocean gliders have demonstrated their effectiveness in meeting these demands, reducing biases from ship-based 'fair weather' sampling and complementing Earth observation capabilities. Future research should explore the seasonality of water column structure and its influence on dissolved oxygen, as well as interactions with current and wind-driven upwelling. A better understanding of these dynamics, including potential feedbacks and tipping points, will support sustainable resource management and provide insights applicable to other western boundary upwelling systems facing the growing threat of deoxygenation (Schulz et al., 2019).

Data availability statement

The CTD survey (doi.org/10.5285/ce27e302-94ec-41ee-e053-6c86abc044c8) and ocean glider data (doi.org/10.5285/d80c6fa6-43ce-2ee1-e053-6c86abc04e3a, doi.org/10.5285/dfdae10d-bb47-4a3b-e053-17d1a68b85ac) used in this work are FAIR compliant and available from the British Oceanographic Data Centre. ERA5 reanalysis data (doi.org/10.24381/cds.adbb2d47) are publicly available and were downloaded from the Copernicus C3S Climate Data Store (https://cds.climate.copernicus.eu/). OSTIA data (doi.org/10.48670/moi-00165) are freely available to download from the CMEMS (http://marine.copernicus.eu).

Author contributions

JW: Data curation, Conceptualization, Writing – review & editing, Writing – original draft, Investigation, Methodology,

Visualization, Formal Analysis. MP: Conceptualization, Investigation, Writing – review & editing, Funding acquisition, Project administration, Data curation, Methodology, Formal Analysis. AP: Writing – review & editing, Conceptualization, Investigation. MN: Data curation, Writing – review & editing. MR: Project administration, Writing – review & editing, Investigation, Conceptualization, Funding acquisition. EP: Conceptualization, Project administration, Funding acquisition, Writing – review & editing.

Funding

The author(s) declared that financial support was received for this work and/or its publication.

Acknowledgments

This work was funded by the UKRI Global Challenges Research Fund under NERC grant NE/P021050. This work was also part of the UK-SA bilateral chair of Ocean Science and Marine Food Security funded by the NRF/DST Grant (98399) and the British Council Newton Fund grant SARCI150326116102/NRF 98399. We thank the officers and crew of the RV *Ellen Kuzwayo*, the South African Department of Agriculture, Forestry and Fisheries (now DEFF) and the UK MARS team for their assistance with data collection. The OSTIA SST data were provided by GHRSST, Met Office and CMEMS. The results contain modified Copernicus Climate Change Service information 2020. Neither the European Commission nor ECMWF is responsible for any use that may be made of the Copernicus information or data it contains. The authors thank the anonymous reviewers who helped improve this manuscript.

Conflict of interest

The author(s) declared that this work was conducted in the absence of any commercial or financial relationships that could be construed as a potential conflict of interest.

Generative AI statement

The author(s) declared that generative AI was used in the creation of this manuscript. Generative AI was used for minor language editing (grammar and flow).

Any alternative text (alt text) provided alongside figures in this article has been generated by Frontiers with the support of artificial intelligence and reasonable efforts have been made to ensure accuracy, including review by the authors wherever possible. If you identify any issues, please contact us.

Publisher's note

Supplementary material

The Supplementary Material for this article can be found online at: https://www.frontiersin.org/articles/10.3389/fmars.2026.1733489/full#supplementary-material.

References

Akpinar, A., Palmer, M. R., Inall, M., Berx, B., and Polton, J. (2022). Locally modified winds regulate circulation in a semi-enclosed shelf sea. *J. Geophysical Research: Oceans* 127 (3), e2021JC018248. doi: 10.1029/2021JC018248

Beal, L. M., and Elipot, S. (2016). Broadening not strengthening of the Agulhas Current since the early 1990s. *Nature* 540, 570–573. doi: 10.1038/nature19853

Beal, L. M., Elipot, S., Houk, A., and Leber, G. M. (2015). Capturing the transport variability of a western boundary jet: Results from the Agulhas Current Time-Series Experiment (ACT). *J. Phys. Oceanogr.* 45, 1302–1324. doi: 10.1175/jpo-d-14-0119.1

Best, M. A., Wither, A. W., and Coates, S. (2007). Dissolved oxygen as a physico-chemical supporting element in the Water Framework Directive. *Mar. Pollut. Bull.* 55 (1-6), 53–64. doi: 10.1016/j.marpolbul.2006.08.037

Bittig, H. C., Fiedler, B., Scholz, R., Krahmann, G., and Körtzinger, A. (2014). Time response of oxygen optodes on profiling platforms and its dependence on flow speed and temperature. *Limnology Oceanography: Methods* 12, 617–636. doi: 10.4319/lom.2014.12.617

Bopp, L., Resplandy, L., Orr, J. C., Doney, S. C., Dunne, J. P., Gehlen, M., et al. (2013). Multiple stressors of ocean ecosystems in the 21st century: projections with CMIP5 models. *Biogeosciences* 10, 6225–6245. doi: 10.5194/bg-10-6225-2013

Boyd, A. J., and Shillington, F. A. (1994). Physical forcing and circulation patterns on the Agulhas Bank. *S. Afr. J. Sci.* 90, 143–154. Available online at: https://hdl.handle.net/10520/AJA00382353_4624.

Boyer, D. C., Boyer, H. J., Fossen, I., and Kreiner, A. (2001). Changes in abundance of the northern Benguela sardine stock during the decade 1990–2000, with comments on the relative importance of fishing and the environment. *Afr. J. Mar. Sci.* 23, 67–84. doi: 10.2989/025776101784528854

Bravo, L., Ramos, M., Astudillo, O., Dewitte, B., and Goubanova, K. (2016). Seasonal variability of the Ekman transport and pumping in the upwelling system off central-northern Chile (~ 30° S) based on a high-resolution atmospheric regional model (WRF). *Ocean Sci.* 12, 1049–1065. doi: 10.5194/os-12-1049-2016

Breitburg, D., Levin, L. A., Oschlies, A., Grégoire, M., Chavez, F. P., Conley, D. J., et al. (2018). Declining oxygen in the global ocean and coastal waters. *Science* 359. doi: 10.1126/science.aam7240

Chapman, P., and Largier, J. L. (1989). On the origin of Agulhas Bank bottom water. *S. Afr. J. Sci.* 85, 515.

Chapman, P., and Shannon, L. V. (1987). Seasonality in the oxygen minimum layers at the extremities of the Benguela system. *South. Afr. J. Mar. Sci.* 5, 85–94. doi: 10.2989/025776187784522162

Chavez, F. P., and Messié, M. (2009). A comparison of eastern boundary upwelling ecosystems. *Prog. Oceanogr.* 83, 80–96. doi: 10.1016/j.pocean.2009.07.032

Chelton, D. B., Schlax, M. G., Freilich, M. H., and Milliff, R. F. (2004). Satellite measurements reveal persistent small-scale features in ocean winds. *Science* 303, 978–983. doi: 10.1126/science.1091901

Claret, M., Galbraith, E. D., Palter, J. B., Bianchi, D., Fennel, K., Gilbert, D., et al. (2018). Rapid coastal deoxygenation due to ocean circulation shift in the northwest Atlantic. *Nat. Clim. Change* 8, 868–872. doi: 10.1038/s41558-018-0263-1

Diaz, R. J., and Rosenberg, R. (2008). Spreading dead zones and consequences for marine ecosystems. *Science* 321, 926–929. doi: 10.1126/science.1156401

Ekau, W., Auel, H., Pörtner, H.-O., and Gilbert, D. (2010). Impact of hypoxia on the structure and processes in pelagic communities (zooplankton, macro-invertebrates and fish). *Biogeosciences* 7, 1669–1699. doi: 10.5194/bg-7-1669-2010

Fennel, K., and Testa, J. M. (2019). Biogeochemical controls on coastal hypoxia. *Annu. Rev. Mar. Sci.* 11, 105–130. doi: 10.1146/annurev-marine-010318-095138

Flynn, R. F., Granger, J., Veitch, J. A., Siedlecki, S., Burger, J. M., Pillay, K., et al. (2020). On-shelf nutrient trapping enhances the fertility of the Southern Benguela upwelling system. *J. Geophysical Research: Oceans* 125, e2019JC015948. doi: 10.1029/2019jc015948

Garau, B., Ruiz, S., Zhang, W. G., Pascual, A., Heslop, E., Kerfoot, J., et al. (2011). Thermal lag correction on Slocum CTD glider data. *J. Atmos. Oceanic Technol.* 28, 1065–1071. doi: 10.1175/jtech-d-10-05030.1

Giering, S. L., Noyon, M., Godfrey, B., Poulton, A. J., Carvalho, F., and Roberts, M. (2022). Optical particle measurements reveal cross-shelf turbidity gradients on the Agulhas Bank. *Deep Sea Res. Part. II: Topical Stud. Oceanography* 200, 105094. doi: 10.1016/j.dsr2.2022.105094

Gill, A. E. (1982). *Atmosphere-ocean dynamics* (Vol. 30). (San Diego: Academic Press).

Good, S., Fiedler, E., Mao, C., Martin, M. J., Maycock, A., Reid, R., et al. (2020). The current configuration of the OSTIA system for operational production of foundation sea surface temperature and ice concentration analyses. *Remote Sens.* 12, 720. doi: 10.3390/rs12040720

Grantham, B. A., Chan, F., Nielsen, K. J., Fox, D. S., Barth, J. A., Huyer, A., et al. (2004). Upwelling-driven nearshore hypoxia signals ecosystem and oceanographic changes in the northeast Pacific. *Nature* 429, 749–754. doi: 10.1038/nature02605

Gregg, M. C., D'Asaro, E. A., Riley, J. J., and Kunze, E. (2018). Mixing efficiency in the ocean. *Annu. Rev. Mar. Sci.* 10, 443–473. doi: 10.1146/annurev-marine-121916-063643

Halpern, D. (2002). Offshore Ekman transport and Ekman pumping off Peru during the 1997–1998 El Nino. *Geophys. Res. Lett.* 29, 19–11. doi: 10.1029/2001gl014097

Hersbach, H., Bell, B., Berrisford, P., Biavati, G., Horányi, A., Muñoz Sabater, J., et al. (2018). "ERA5 hourly data on single levels from 1979 to present," in *Copernicus Climate Change Service (C3S), Climate Data Store (CDS).* (ECMWF, Reading). doi: 10.24381/cds.adbb2d47

Hickman, A. E., Moore, C. M., Sharples, J., Lucas, M. I., Tilstone, G. H., Krivtsov, V., et al. (2012). Primary production and nitrate uptake within the seasonal thermocline of a stratified shelf sea. *Mar. Ecol. Prog. Ser.* 463, 39–57. doi: 10.3354/meps09836

Hutchings, L. (1994). The Agulhas Bank: a synthesis of available information and a brief comparison with other east-coast shelf regions. *S. Afr. J. Sci.* 90, 179–185. Available online at: https://hdl.handle.net/10520/AJA00382353_4628.

Jackson, J. M., Rainville, L., Roberts, M. J., McQuaid, C. D., and Lutjeharms, J. R. (2012). Mesoscale bio-physical interactions between the Agulhas Current and the Agulhas Bank, South Africa. *Cont. Shelf Res.* 49, 10–24. doi: 10.1016/j.csr.2012.09.005

Jebri, F., Raitsos, D. E., Gittings, J. A., Jacobs, Z. L., Srokosz, M., Gornall, J., et al. (2022). Unravelling links between squid catch variations and biophysical mechanisms in South African waters. *DSR II: Topical Stud. Oceanography* 196, 105028. doi: 10.1016/j.dsr2.2022.105028

Jury, M. R. (2020). Marine climate change over the eastern Agulhas Bank of South Africa. *Ocean Sci.* 16, 1529–1544. doi: 10.5194/os-16-1529-2020

Kara, A. B., Wallcraft, A. J., Metzger, E. J., Hurlburt, H. E., and Fairall, C. W. (2007). Wind stress drag coefficient over the global ocean. *J. Clim.* 20, 5856–5864. doi: 10.1029/2006gl027849

Krug, M., and Penven, P. (2011). New perspectives on Natal Pulses from satellite observations. *J. Geophysical Research: Oceans* 116. doi: 10.1029/2010jc006866

Krug, M., Tournadre, J., and Dufois, F. (2014). Interactions between the Agulhas Current and the eastern margin of the Agulhas Bank. *Cont. Shelf Res.* 81, 67–79. doi: 10.1016/j.csr.2014.02.020

Langdon, C. (2010). "Determination of dissolved oxygen in seawater by Winkler titration using the amperometric technique," in *International Ocean Carbon Coordination Project Report No. 14, International CLIVAR Project Office Publication Series No. 134, Version 1.* (Paris: UNESCO), 1–18. doi: 10.25607/OBP-1350

Largier, J. L., and Swart, V. P. (1987). East-west variation in thermocline breakdown on the Agulhas Bank. *South. Afr. J. Mar. Sci.* 5, 263–272. doi: 10.2989/025776187784522252

Leber, G. M., Beal, L. M., and Elipot, S. (2017). Wind and current forcing combine to drive strong upwelling in the Agulhas Current. *J. Phys. Oceanogr.* 47, 123–134. doi: 10.1175/jpo-d-16-0079.1

Lovecchio, E., Henson, S., Carvalho, F., and Briggs, N. (2022). Oxygen variability in the offshore northern Benguela Upwelling System from glider data. *J. Geophysical Research: Oceans* 127, e2022JC019063. doi: 10.1029/2022jc019063

Lueck, R. G., and Picklo, J. J. (1990). Thermal inertia of conductivity cells: Observations with a Sea-Bird cell. *J. Atmos. Oceanic Technol.* 7, 756–768. doi: 10.1175/1520-0426(1990)007<0756:tiocco>2.0.co;2

Lutjeharms, J. R. E., Meyer, A. A., Ansorge, I. J., Eagle, G. A., and Orren, M. J. (1996). The nutrient characteristics of the Agulhas Bank. *S. Afr. J. Mar. Sci.* 17 (1), 253–274. doi: 10.2989/025776196784158464

Lutjeharms, J. R. E., Cooper, J., and Roberts, M. (2000). Upwelling at the inshore edge of the Agulhas Current. *Cont. Shelf Res.* 20, 737–761. doi: 10.1016/s0278-4343(99)00092-8

Luyten, J., Pedlosky, J., and Stommel, H. (1983). Climatic inferences from the ventilated thermocline. *Clim. Change* 5, 183–193. doi: 10.1007/bf02423489

MacKinnon, J. A., and Gregg, M. C. (2005). Spring mixing: Turbulence and internal waves during restratification on the New England shelf. *J. Phys. Oceanogr.* 35, 2425–2443. doi: 10.1175/jpo2821.1

Mahaffey, C., Palmer, M., Greenwood, N., and Sharples, J. (2020). Impacts of climate change on dissolved oxygen concentration relevant to the coastal and marine environment around the UK. *MCCIP Sci. Rev.* 2002, 31–53. doi: 10.14465/2020.arc02.oxy

Malan, N., Backeberg, B., Biastoch, A., Durgadoo, J. V., Samuelsen, A., Reason, C., et al. (2018). Agulhas Current Meanders facilitate shelf-slope exchange on the Eastern Agulhas Bank. *J. Geophysical Research: Oceans* 123, 4762–4778. doi: 10.1029/2017jc013602

Mazwane, S. L., Poulton, A. J., Hickman, A. E., Jebri, F., Jacobs, Z., Roberts, M., et al. (2022). Spatial and temporal variability of Net Primary Production on the Agulhas Ban–2018. *Deep Sea Res. Part. II: Topical Stud. Oceanography* 199, 105079. doi: 10.1016/j.dsr2.2022.105079

Monismith, S. G., Koseff, J. R., and White, B. L. (2018). Mixing efficiency in the presence of stratification: When is it constant? *Geophys. Res. Lett.* 45, 5627–5634. doi: 10.1029/2018GL077229

Moore, C. M., Suggett, D., Holligan, P. M., Sharples, J., Abraham, E. R., Lucas, M. I., et al. (2003). Physical controls on phytoplankton physiology and production at a shelf sea front: a fast repetition-rate fluorometer based field study. *Mar. Ecol. Prog. Ser.* 259, 29–45. doi: 10.3354/meps259029

Noyon, M. (2019). *Ellen Khuzwayo EK188 – cruise summary report, Version 2.* (Liverpool: British Oceanographic Data Centre (BODC)), 61. Available online at: https://www.bodc.ac.uk/resources/inventories/cruise_inventory/reports/ellenkhuzwayo_188.pdf (Accessed March 2022).

Osborn, T. R. (1980). Estimates of the local rate of vertical diffusion from dissipation measurements. *J. Phys. Oceanogr.* 10, 83–89. doi: 10.1175/1520-0485(1980)010<0083:eotlro>2.0.co;2

Oschlies, A., Brandt, P., Stramma, L., and Schmidtko, S. (2018). Drivers and mechanisms of ocean deoxygenation. *Nat. Geosci.* 11, 467–473. doi: 10.1038/s41561-018-0152-2

OSPAR (2017). "Eutrophication Status of the OPSAR Maritime Area." in *Third Integrated report on the Eutrophication Status of the OPSAR Maritime Area. Eutrophication Series* (London: OSPAR Commission), 164.

Painting, S. J., Devlin, M. J., Rogers, S. I., Mills, D. K., Parker, E. R., and Rees, H. L. (2005). Assessing the suitability of OSPAR EcoQOs for eutrophication vs ICES criteria for England and Wales. *Mar. pollut. Bull.* 50, 1569–1584. doi: 10.1016/j.marpolbul.2005.06.042

Palmer, M. R., Stephenson, G. R., Inall, M. E., Balfour, C., Düsterhus, A., and Green, J. A. M. (2015). Turbulence and mixing by internal waves in the Celtic Sea determined from ocean glider microstructure measurements. *J. Mar. Syst.* 144, 57–69. doi: 10.1016/j.jmarsys.2014.11.005

Pickett, M. H., and Paduan, J. D. (2003). Ekman transport and pumping in the California Current based on the US Navy's high-resolution atmospheric model (COAMPS). *J. Geophysical Research: Oceans* 108. doi: 10.1029/2003jc001902

Poulton, A. J., Mazwane, S. L., Godfrey, B., Carvalho, F., Mawji, E., Wihsgott, J. U., et al. (2022). Primary production dynamics on the Agulhas Bank in autumn. *DSR II: Topical Stud. Oceanography* 203, 105153. doi: 10.1016/j.dsr2.2022.105153

Probyn, T. A., Mitchell-Innes, B. A., Brown, P. C., Hutchings, L., and Carter, R. (1994). A review of primary production and related processes on the Agulhas Bank. *S. Afr. J. Sci.* 90, 166–173. Available online at: https://hdl.handle.net/10520/AJA00382353_4632.

Qian, W., Dai, M., Xu, M., Kao, S. J., Du, C., Liu, J., et al. (2017). Non-local drivers of the summer hypoxia in the East China Sea off the Changjiang Estuary. *Estuar. Coast. Shelf Sci.* 198, 393–399. doi: 10.1016/j.ecss.2016.08.032

Rippeth, T., Shen, S., Lincoln, B., Scannell, B., Meng, X., Hopkins, J., et al. (2024). The deepwater oxygen deficit in stratified shallow seas is mediated by diapycnal mixing. *Nat. Commun.* 15, 3136. doi: 10.1038/s41467-024-47548-2

Roberts, M. J. (2005). Chokka squid (Loligo vulgaris reynaudii) abundance linked to changes in South Africa's Agulhas Bank ecosystem during spawning and the early life cycle. *ICES J. Mar. Sci.* 62, 33–55. doi: 10.1016/j.icesjms.2004.10.002

Rykaczewski, R. R., and Checkley, D. M. (2008). Influence of ocean winds on the pelagic ecosystem in upwelling regions. *Proc. Natl. Acad. Sci.* 105, 1965–1970. doi: 10.1073/pnas.0711777105

Schmidtko, S., Stramma, L., and Visbeck, M. (2017). Decline in global oceanic oxygen content during the past five decades. *Nature* 542, 335–339. doi: 10.1038/nature21399

Schulz, K. G., Hartley, S., and Eyre, B. (2019). Upwelling amplifies ocean acidification on the East Australian Shelf: Implications for marine ecosystems. *Front. Mar. Sci.* 6, 636. doi: 10.3389/fmars.2019.00636

Sharples, J., Moore, M. C., Rippeth, T. P., Holligan, P. M., Hydes, D. J., Fisher, N. R., et al. (2001). Phytoplankton distribution and survival in the thermocline. *Limnol. Oceanogr.* 46, 486–496. doi: 10.4319/lo.2001.46.3.0486

Steckbauer, A., Duarte, C. M., Carstensen, J., Vaquer-Sunyer, R., and Conley, D. J. (2011). Ecosystem impacts of hypoxia: thresholds of hypoxia and pathways to recovery. *Environ. Res. Lett.* 6, 25003. doi: 10.1088/1748-9326/6/2/025003

Stramma, L., Johnson, G. C., Sprintall, J., and Mohrholz, V. (2008). Expanding oxygen-minimum zones in the tropical oceans. *Science* 320, 655–658. doi: 10.1126/science.1153847

Swart, V. P., and Largier, J. L. (1987). Thermal structure of Agulhas Bank water. *South. Afr. J. Mar. Sci.* 5, 243–252. doi: 10.2989/025776187784522153

Townsend, D. W., Thomas, A. C., Mayer, L. M., Thomas, M. A., and Quinlan, J. A. (2006). "Oceanography of the northwest Atlantic continental shelf," in *The Sea: The Global Coastal Ocean. Interdisciplinary Regional Studies and Syntheses*, vol. 14, eds. A. R. Robinson and K. H. Brink. (Cambridge, MA: Harvard University Press), 119–168.

Vaquer-Sunyer, R., and Duarte, C. M. (2008). Thresholds of hypoxia for marine biodiversity. *Proc. Natl. Acad. Sci.* 105, 15452–15457. doi: 10.1073/pnas.0803833105

Wang, Y., and Castelao, R. M. (2016). Variability in the coupling between sea surface temperature and wind stress in the global coastal ocean. *Cont. Shelf Res.* 125, 88–96. doi: 10.1016/j.csr.2016.07.011

Waterhouse, A. F., MacKinnon, J. A., Nash, J. D., Alford, M. H., Kunze, E., Simmons, H. L., et al. (2014). Global patterns of diapycnal mixing from measurements of the turbulent dissipation rate. *J. Phys. Oceanogr.* 44, 1854–1872. doi: 10.1175/jpo-d-13-0104.1

Wei, Q., Yao, Q., Wang, B., Xue, L., Fu, M., Sun, J., et al. (2019). Deoxygenation and its controls in a semienclosed shelf ecosystem, northern Yellow Sea. *J. Geophysical Research: Oceans* 124, 9004–9019. doi: 10.1029/2019jc015399

Williams, C. A. J., Davis, C. E., Palmer, M. R., Sharples, J., and Mahaffey, C. (2022). The three rs: resolving respiration robotically in shelf seas. *Geophys. Res. Lett.* 49, e2021GL096921. doi: 10.1029/2021gl096921

Yu, L., Fennel, K., and Laurent, A. (2015). A modeling study of physical controls on hypoxia generation in the northern Gulf of Mexico. *J. Geophysical Research: Oceans* 120, 5019–5039. doi: 10.1002/2014jc010634